2023 IEEE International Conference on Robotics and Automation (ICRA 2023)
May 29 - June 2, 2023. London, UK

Contact Based Turning Gait of a Novel Legged-Wheeled Quadruped

Alper Yeldan, Abhimanyu Arora, Gim Song Soh

***Abstract*— How does a wheeled robot move and turn? The answer is straightforward for a conventional wheeled robot, but it is not so easy for a robot with a discrete wheel design. Regular wheeled robots always have four contact points, resulting in static stability during locomotion. However, QuadRunner's novel leg mechanism provides only a semi-circular wheel shape, and proper gait planning is needed to go straight or turn. Therefore, this paper presents a dual frequency gait planning method which controls the robot's gait cycle's duty factor and generates unique turning gait patterns for wheel locomotion. Describing requirements and limitations, we found sets of solutions that can achieve turning. Results show that the smallest turning radius QuadRunner achieved is $1.05m$, and the biggest is $1.86m$. In addition, detailed experiments were made to observe the performance and stability of straight and turning wheel behaviors. Finally, a gait verification is made using high-speed cameras.**

I. Introduction

The presence of mobile robots is ever-increasing; they are used in various fields, such as exploration, search and rescue, object handling, and inspection [1]. Although legged robots can climb obstacles, they require complex mechanical and control systems. Wheeled robots, on the other hand, have simple designs and provide efficient, smooth, and fast locomotion on flat surfaces. Its dynamics can be significantly simplified by using three or more wheels, making the robot statically stable. Thus, many mobile robots integrate wheeled locomotion into their systems to create legged-wheeled systems. Robots that use wheel locomotion should also be able to avoid obstacles, which is done via a turning behavior. Turning can be made as either a zero-turn or steer with a turning radius. A robot's ability to turn is essential to its maneuverability and should be implemented correctly to get the highest output.

Wheeled robots commonly achieve turning with differential drive [2] where the actuator speed of one side of the robot is different from the other. Therefore several robots with differing sizes but similar kinematic models can be found in the literature [3]–[6]. The same cannot be said for legged-wheeled robots since legs and wheels can be combined differently depending on the task at hand. Thus, there is no 'correct' method to create legged-wheeled robots, and each has performed turning based on their kinematic and dynamic limitations. For example, OctaRoach [7] attached a low-mass tail to its body to achieve fast and reliable turning along with its existing differential drive capabilities. With these systems combined, the robot can turn up to $400°/sec$. Talbot [8] is a tracked-legged transformable robot that uses a novel switch mechanism and control strategy to move in rugged terrains efficiently. When the robot is in the tracked mode, it is controlled by a tracked foot differential on both sides. In Rhex [9], turning during translation is achieved by introducing differential perturbations to straight locomotion parameters for contralateral legs. This way gait cycle period stays the same for all legs while altering leg offset and swing time. Turboquad [10] adds a Watt's six-bar linkage with parameters selected to approximately behave like Ackermann's steering principle, allowing it to turn up to 12° without colliding with its body. Rover type of quadruped wheeled robots [11]–[13] can traverse rugged environment by using their legged mechanism as a passive suspension mechanism that adapts to the terrain variations and maintain desired body pose. Each leg has an actuator to steer the wheel and accomplish reliable slow-speed driving. Lywall [14] is a transformable leg-wheel robot whose 5-bar leg design allows it to switch between wheel, leg, and claw modes. When its legs are put into a specific orientation, the arcs attached to its legs form a circle, allowing Lywall to act as a differential wheeled robot. Claw-wheel robot [15] controls a pitch joint

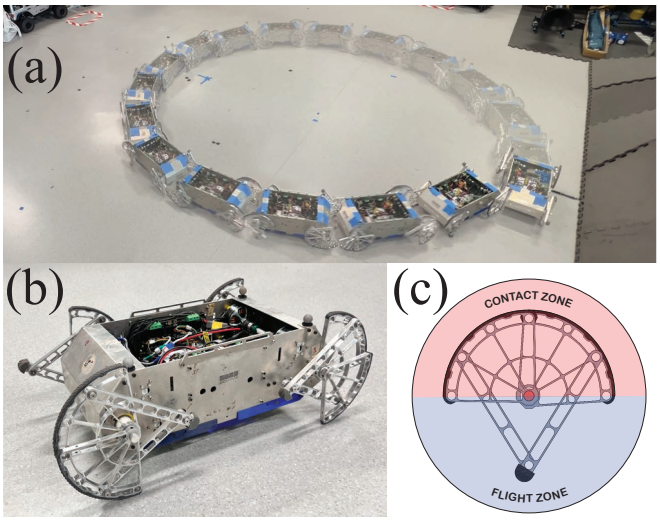

Fig. 1: (a) QuadRunner turning wheel locomotion. A video recording of the experiments can be found at https://tinyurl.com/QuadRunnerTurning. (b) QuadRunner in wheel mode. (c) Dual frequency gait cycle zones.

The authors are with the Singapore University of Technology and Design, Engineering Product Development Pillar, Singapore sohgimsong@sutd.edu.sg

that folds the robot when wheel locomotion is desired. S-shaped legs complement each other and form a full circle when the robot is folded. Thus, the robot becomes a 2-wheeled differential drive robot with a ball caster. Recently, a semi-circular wheeled robot [16] was developed where it executes zero-turns by adjusting leg phases. It also turns using a crawl gait, but it has a large turning radius, $2.89m$, and significantly slow in its current state.

In general, wheeled robots (and hybrid robots with wheels) can realize stable locomotion with full-circle wheels; however, this is not directly possible for QuadRunner. As shown in Fig.1, wheeled locomotion can happen when wheels are in a specific configuration, and each wheel can only contact the ground half of the time because of its semi-circular area. Thus, gait planning is needed to overcome this limitation. It has been shown in [17] that linear wheeled locomotion can be achieved by maintaining certain phases between legs. However, if the robot tries to turn by applying different velocities to its left and right side, the phases between legs would not remain constant, which results in the robot's falling when none of the semi-circular contact areas are in contact. This paper presents a new gait planning method that allows QuadRunner to turn while satisfying stability requirements. Stability of the robot is analyzed based on number of wheel contacts during locomotion. Static stability obtained by having at least 3 wheel contacts, whereas dynamic stability can be achieved when there is only two diagonally contacts. Robot stability is achieved by applying different frequencies during 'contact' and 'flight' zones, which changes the contact percentage of the gait cycle. In the following, we present QuadRunner's design, characterization, and implementation of dual frequency gait planning for all types of wheel locomotion.

II. Robot Design

QuadRunner is a transformable quasi-wheel quadruped, where the leg and wheel geometry is embedded into a 5-bar linkage. When put in a specific pose, each leg forms a semicircular wheel shape that acts as a contact area in wheeled locomotion along with the end-effector. Detailed robot design and locomotion transition strategies can be found in [17].

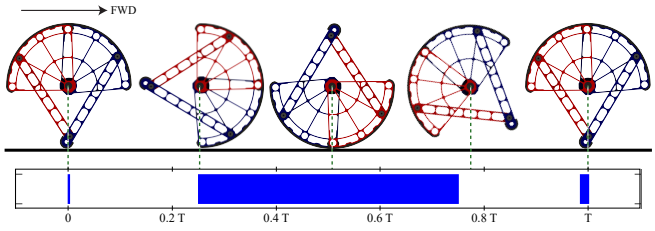

Fig. 2: (a) Pose of the QuadRunner's leg while completing 1 revolution in constant angular velocity. (b) Gait diagram of the leg. Green dashed lines shows whether leg is in contact at that pose.

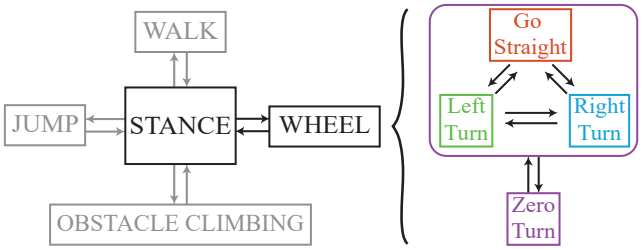

Fig. 3: QuadRunner's state machine. Wheel locomotion divide into behaviors. Arrows indicate possible mode changes. Every behavior except zero-turn starts with the same leg phases, thus robot can switch between them directly.

In Fig.2, one of QuadRunner's legs is actuated and completes one revolution, and its corresponding gait diagram is depicted. Blue areas in the gait diagram indicate that leg is in contact with the ground, whereas white areas imply the flight phase. T is the period of locomotion, which can be calculated using angular velocity and the wheel radius of the leg. The duty factor (DT), which is the percentage of contact time of this gait cycle, can be expressed as

$$DT = cp\% + cp_{end}\% \tag{1}$$

where $cp\%$ and $cp_{end}\%$ are the duty factors of semi-circle and end-effector contact areas, respectively. Since the semi-circle wheel is half of the whole revolution, $cp\% = 50\%$, and based on geometry, cp_{end} is calculated as 3% when the wheel rotates at a constant speed.

QuadRunner's state machine is shown in Fig.3, where arrows indicate feasible changes between modes. For example, a conventional wheeled robot can turn and move straight since it is not constrained by contact stability. However, due to its wheel geometry, QuadRunner has to divide wheeled behaviors into different states and analyze them separately. In order to transition between wheel behaviors seamlessly, a constraint of having the same initial phase between wheels for all-wheel sub-states is imposed, which eliminates the transition procedure. However, zero-turn behavior has a specific phase offset that needs to be obtained when switching from other wheel behaviors.

III. Turning Gait Strategy

A. Dual Frequency Gait Cycle

Although QuadRunner's leg design allow robot to achieve wheel locomotion without any extra actuators or the wheel itself, it complicates the locomotion and add limitations to the system. Since its wheels don't contact with the ground (even in flat surface) throughout the locomotion, it is more prone fail against external disturbances, thus has lower stability, compared to robots with 4 wheels. This problem can be solved by increasing the DT of each limb. When QuadRunner's limbs are in flight, they do not contribute to the wheeled locomotion. This means that the velocity can be

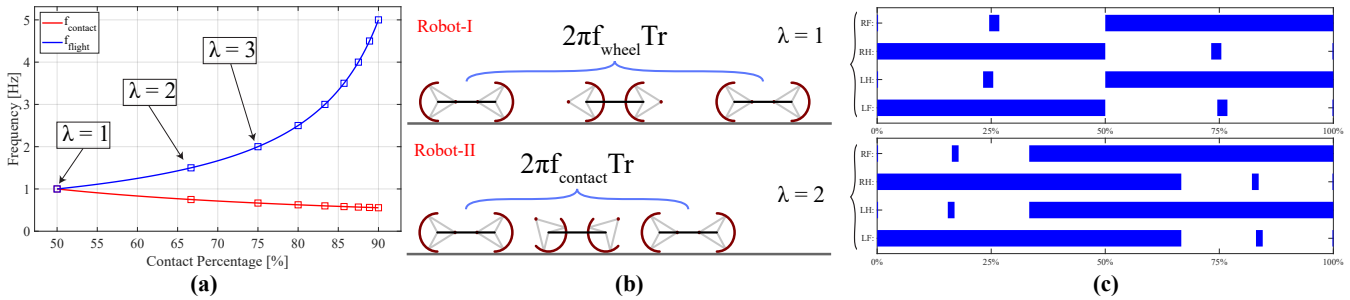

Fig. 4: (a) Flight and contact frequency values of a wheel with different contact percentages, where $f_{wheel} = 1Hz$. Boxes indicate particular frequencies for integer values of λ. (b) Simulation of 1 gait cycle of QuadRunner with the same f_{wheel}, but different λ values. (c) Respective gait diagram of the simulated robots.

changed independently during their respective flight phases. Based on this idea, a dual frequency wheeled locomotion is implemented, where the limb during wheeled configuration is divided into two zones, namely contact and flight, shown in Fig.1(c). When the limb is in the contact zone, it revolves at a slower speed, which increases the contact time during the gait cycle. Then, the same limb should turn faster when in the flight zone to maintain a given gait cycle period, completing one full revolution of the wheel. Thus, DT of the limb is increased.

One revolution of the wheel can be expressed as

$$\theta_{wheel} = \theta_{contact} + \theta_{flight} \tag{2}$$

where $\theta_{contact}$ is the angular distance covered while the leg's semi-circular link is in contact and θ_{flight} is the distance traversed while leg has no contact with the ground. It should be noted that the end-effector is within the flight zone and contacts the ground at flight frequency. Although this contact at a higher speed may cause perturbations in the gait cycle, since $cp_{end}\%$ is significantly smaller than $cp\%$, the effect of the end-effector contact is neglected. Regardless, the end-effector is considered as a contact point when the stability during locomotion is analyzed. The frequency of the wheel in the contact and flight zones are $f_{contact}$ and f_{flight}, respectively. Then, Eq.2 can be described as

$$\begin{aligned} 2\pi f_{wheel} \cdot T = {} & 2\pi f_{contact} \cdot T \cdot cp\% \\ & + 2\pi f_{flight} \cdot T \cdot (1 - cp\%) \end{aligned} \tag{3}$$

where f_{wheel} is the average gait cycle frequency of the leg. This means that $cp\%$ can be changed without varying QuadRunner's gait cycle period. It also implies that the angular frequency of the wheel locomotion is $f_{contact}$. As seen in Fig.1(c), contact and flight zones are divided equally. Thus,

$$\theta_{contact} = \theta_{flight} \tag{4}$$

substituting the frequencies used in the respective zones, the equation can be described as

$$2\pi f_{contact} \cdot T \cdot cp\% = 2\pi f_{flight} \cdot T \cdot (1 - cp\%) \tag{5}$$

which simplifies to

$$\frac{f_{flight}}{f_{contact}} = \frac{cp\%}{1 - cp\%} = \lambda \tag{6}$$

where λ is the ratio between frequencies, and used to set $cp\%$ of the gait cycle.

Using the equations above, a plot of the resulting flight and contact frequency values for a desired contact percentage is presented in Fig.4(a). The red curve is $f_{contact}$, blue curve is f_{flight}, and f_{wheel} is set as $1Hz$. When λ is 1, wheels rotate at the same speed in both zones resulting in a $cp\%$ of 50%. On the other hand, when the leg has 75% contact during its gait cycle, its flight frequency is three times its contact frequency. It is observed that as contact percentage increases, flight frequency increases exponentially. Attempting to instantly change the actuators' frequency by such a large value can result in large overshoots and poor tracking of the desired gait. It may also result in large vibrations as $cp\%$ increases. Experiments on QuadRunner suggest that λ should be lower than 4 to obtain reliable wheeled locomotion.

Shown in Fig.4(b), a simulation is carried out to visualize the execution of the dual frequency gait cycle method. Both of the robots were configured to have the same wheel phases, and f_{wheel} is specified as $1Hz$. The only difference is the λ of the robots, with values of 1 and 2, respectively. The distance traveled by one gait cycle can be calculated as $2\pi fTr$,where r is the wheel radius and $10cm$. Using f_{wheel}, the period is calculated as $1sec$. In Robot-I, $f_{contact}$ is the same as f_{wheel}, since λ is 1. However, in Robot-II $f_{contact}$ is $0.75Hz$ and not the same as f_{wheel}. Therefore, the robots traveled different distances for the same duration. Additionally, the gait diagrams of the simulated robots are shown in Fig.4(c), where each colored box indicates the duration that the leg is in contact with the ground. Robot-I obtains static stability only when the end-effectors are in contact with the ground, which is for 8.6% of the gait cycle. On the other hand, there are regions where all the semi-circular contact areas of the Robot-II touch the ground together, gaining extra static stability for a total of 39.7% of the gait cycle.

B. Defining Turning Gait in Semi-Circle Wheel

In order to achieve a gait [18], each limb must complete its cycle in the same length of time, which preserves the phase difference between limbs and allows robots to execute the same pattern repeatedly. To create a successful turning gait in QuadRunner, two conditions must be met. First, the parameters chosen for turning must result in a gait cycle with a reasonable period. Secondly, during this gait cycle, the robot's stability needs to be analyzed since each limb does not have constant contact with the ground. First, the turning gait cycle period T is calculated by defining left and right angular frequencies of the robot f_L and f_R, respectively. Then, the gait cycle period can be calculated as

$$T = lcm\left(\frac{1}{f_L}, \frac{1}{f_R}\right) \tag{7}$$

where calculated, using least common multiplier, T allows each side of the wheel to have any frequency value. Next, amount of revolutions of the wheels on each side required to achieve a complete gait cycle is described as n and calculated as

$$n_i = \frac{T}{f_i}, \quad i \in \{L, R\} \tag{8}$$

where $n_i \in \mathbb{Z}$. For example, if $f_L = 1$ and $f_R = 3$, the robot will steer left with a gait cycle. Period $T = 1sec$ is calculated using Eq.7. Similarly, using Eq.8, the revolution amounts are found as $n_L = 1$ and $n_R = 3$. This means that in one turning gait cycle, the wheels on the left side will complete 1 full revolution, whereas the wheels on the right will fully rotate 3 times.

The last criterion that needs to be satisfied is the robot's stability condition during locomotion. At any point in turning robot is considered stable if:

1) Static stability: There are at least 3 wheels in contact.
2) Dynamic stability: There are two contacts in cross configuration ($\{LF - RH\}$ or $\{LH - RF\}$) and not at the beginning or end of the gait cycle.

In this context, dynamic stability achieved when QuadRunner is not staying stationary and has only 2 diagonal contact points. This stability has already been proven in [17] and a similar method is used to achieve Trot gait in legged locomotion.

C. Turning Gait Library

In order to find successful gait parameters a kinematic simulation is made by sweeping parameters within determined limits. These input parameters and their respective ranges are:

$$g(x) = \begin{cases} f_L, f_R(i) & \in [0 : 0.25 : 4) \\ \phi_{LF}, \phi_{LH} & \in [0 : 0.25 : 1) \\ \lambda_L, \lambda_R) & \in [1 : 0.25 : 4) \end{cases} \tag{9}$$

where ϕ is the initial phase angle of the wheel. There are only 2 phase values, since wheels needs to be diagonally symmetrical as explained in Sect.II. Using these 6 input parameters simulations were performed and several solutions were found. One of the solutions is shown in Fig.5, where the contact duration for each wheel and the stability result are shown. The parameters of the solution are $f_L = 0.5Hz$ and $f_R = 1Hz$, $\lambda_L = 2.25$ and $\lambda_R = 1.75$, and $\phi_{LF} = 0.75$ and $\phi_{LH} = 0.25$. Additionally, the robot is in static stability for 68.8% of the gait cycle. It should be noted that the robot has 4 contact points for the first and last points of the gait cycle, satisfying condition for static stability.

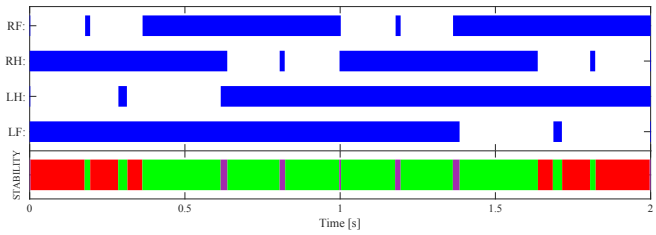

Fig. 5: A solution in gait library where contact and stability diagrams are shown. In stability diagram red color indicates 2 wheel contacts with cross configuration, green color implies 3 wheel contacts, and purple color means all wheels are in contact with ground.

Although steering is important in a robot's maneuverability, another important capability is zero-turn behavior, where actuators on each side of the robot turns in the opposite direction. Possible gait solutions shows that zero-turn is not possible when $\phi_{LF} = 0.75$ and $\phi_{LH} = 0.25$, for which many of the steering solutions exist. Nonetheless, QuadRunner can do a zero-turn when phases are 0 and 0.5 (or vice versa), respectively. This phase pair is only an offset of a quarter of rotation of each wheel. Hence, the robot can switch from other wheel behaviors to zero-turn by moving quarter rotation forwards or backwards.

IV. RESULTS

For analysis of the proposed dual frequency gait cycle method, the various wheel state behaviors in Fig.3 are evaluated separately. Experiments are run with the same parameters as those of the simulated cases discussed thus far to easily allow the reader to compare theoretical and actual results. An OptiTrack motion capture system is used to record the 3D Cartesian coordinates of the robot body during the experiments. The actual and desired position commands, and resulting motor torques are concurrently recorded on an on-board SD card.

A. Straight Locomotion Evaluation

From the motion capture data, the robot's linear velocity is calculated for 5 gait cycles of wheeled locomotion, whose results are seen in Fig.6. Both experiments use the same wheel frequency ($1Hz$) and phase parameters ($0.75, 0.25$), but differing λ values of 1 and 2 for Experiments-I/II respectively.

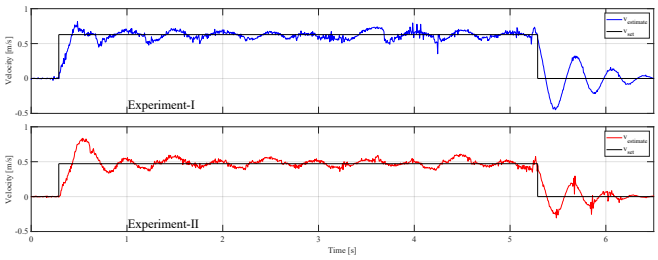

Fig. 6: Linear velocity versus time plot. Both figure have executed 5 gait cycles with average frequency of $1Hz$. Top figure's frequency ratio λ is 2, whereas this value is 1 for the bottom one. Black lines (f_{set}) indicate desired frequency commands, whereas blue (LF) and red (LH) colored lines are estimated values.

The mean velocity error during wheeled locomotion for Experiment-I is 6.7%, and higher at 8.6% for Experiment-II. The main source of the error comes when the robot first starts to move because of the instantaneous speed change. The current method of wheeled locomotion applies desired velocities as a step function which results in oscillations and an increased system error when the robot tries to change its speed in a very short time. Integrating the area below the velocity graphs allows the linear distance traveled to be calculated. Based on the given commands, QuadRunner is supposed to move $31.4cm$ and $23.6cm$ for Experiments-I/II, respectively. Data from motion capture reveals that the robot traveled $30.9cm$ for the first experiment and $24.3cm$ for the second one. The excessive initial oscillation of robot's velocity resulted in the overshoot in position observed in Experiment-II. On the contrary, large oscillations observed at the end of Experiment-I may have caused the robot to slide backward, resulting in the discrepancy.

In continuation of the straight wheeled-locomotion experiment, the frequencies of one of the wheels, LF, during Experiment-II are graphed in Fig.7. The effects of the dual frequency cycle method can be observed as well. Since $\lambda = 2$, f_c and f_f are determined to be $0.75Hz$ and $1.5Hz$. At the start of the gait cycle, LF is at the beginning of its semi-circular contact regions since it has a phase of 0.75. Thus, LF rotates with a frequency of f_c initially. This instant change in velocity produces oscillations which are also observed when the wheel transits to flight phase and

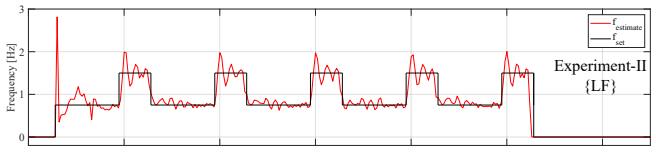

Fig. 7: Frequency plot of wheel LF versus time in a 5 gait cycle straight wheeled locomotion. Data is taken from the Experiment-II shown in Fig.6.

the frequency is set to f_f. As a result, during this first gait cycle, there is an error in the velocity tracking of 24.4%. This reduces to 10.1% in the subsequent gait cycles. It is also observed that oscillations during the contact zones are lower in amplitude compared to while the wheel is in flight. This may be because friction between the wheel and ground provides additional damping allowing for a better response of the actuators' position controllers (when the wheel is in contact with the ground) and, thus, lower error.

B. Turning Locomotion Evaluation

Stability of the robot while turning is examined by estimating the robot's attitude using motion capture data. In Fig.8, QuadRunner's turning wheeled-locomotion on a flat surface is shown. The robot completes 20 gait cycle with an average speed of $0.4m/s$. Using the Taubin circle fitting method, the turn radius is calculated to be $1.78m$. The average error in radius is 2.7%, with a maximum of 6.7%. The periodic nature of QuadRunner's gait cycle is observable in both roll and pitch angles. In the experiment, the highest roll angle measured is $9.2°$ and a lower value of $8°$ for pitch. These results show that QuadRunner can successfully track a circular trajectory, but the small change in turning radius (visible in Fig.8) can be attributed to instant speed change in the beginning of the experiment. This result with undesired sliding of the robot body, but the effects are considered negligible.

Due to the absence of foot contact sensors, direct verification of wheel contacts is not possible. However, by using footage obtained from two high-speed cameras at $240Hz$, a manual estimation is done. The locomotion parameters used are the same as Figures 5 and 8, giving readers a complete analysis of the presented novel method. In Fig.9, the gait diagram of a single cycle is presented from the middle of the recorded data. This ensures that the effects of the instant speed changes that happen at the beginning and end of a gait cycle are not observed. Although QuadRunner generally follows the desired gait cycle, some discrepancies happened during locomotion. In LH and LF, the robot loses contact in the middle of its semi-circular contact region for at least 10% of the gait cycle implying that the robot sways significantly towards both sides during locomotion

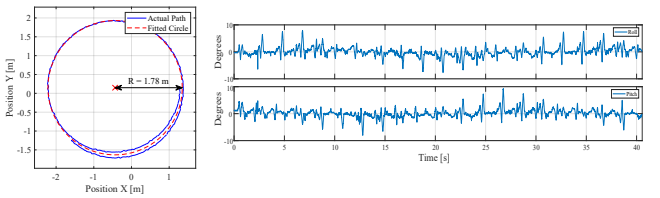

Fig. 8: Turning locomotion of QuadRunner using a solution from the gait library ($[f_L, f_R] = [0.5, 1]Hz$, $[\lambda_L, \lambda_R] = [2.25, 1.75]$, and $[\phi_{LF}, \phi_{LH}] = [0.75, 0.25]$). On the right, roll and pitch angle of the robot are shown.

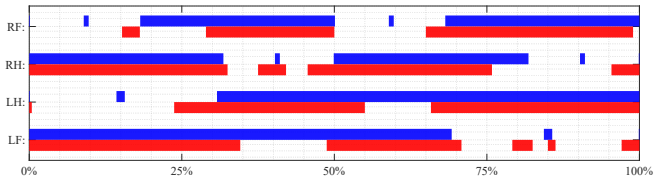

Fig. 9: One gait cycle of turning gait for QuadRunner. Blue color diagram displays the ideal gait, while red color diagram is estimated from camera recordings. Gait parameters are taken from Fig.8.

TABLE I: Turning Gait Library

	Input			Output	
i	f_L, f_R	λ_L, λ_R	ϕ_{LF}, ϕ_{LH}	Radius (R)	Frequency Ratio
$\{1\}$	0.50, 1.00	2.25, 1.75	0.75, 0.25	1.78	2.18
$\{2\}$	0.50, 1.00	2.00, 2.00	0.75, 0.25	1.86	2.00
$\{3\}$	0.25, 0.50	2.00, 2.00	0.75, 0.25	1.69	2.00
$\{4\}$	0.50, 1.50	3.50, 2.00	0.75, 0.25	1.25	3.50
$\{5\}$	0.50, 1.50	3.25, 2.50	0.75, 0.25	1.16	3.21
$\{6\}$	0.25, 0.75	3.25, 2.50	0.75, 0.25	1.05	3.21

as evidenced by the spikes in roll and pitch seen in Fig.8. However, a gait planning method where robot dynamics are also considered can solve the aforementioned problem to achieve better wheeled performance.

C. Modeling Wheeled Locomotion

Table I shows several solutions that can generate successful turning locomotions. The outputs of these solutions are the resulting turning radius and frequency ratio. The frequency ratio is that of $f_{contact,L}$ and $f_{contact,R}$, which are calculated using Eq.6, and required to find the trajectory of the robot as discussed below. Although other solutions with different phases exist, most have a phase pair of $[0.75, 0.25]$. Hence, all cases presented in this paper use this phase pair to simplify the experimental procedure and reduce the variables at hand.

An extended differential-drive skid-steering can be used to model [3], [19] the robot during wheeled locomotion, which suggests that the estimated speed of the robot in its local frame $\hat{\dot{x}} = [v_x, v_y, \omega]^T$, can be expressed as

$$\hat{\dot{x}} = J(u)\Gamma \tag{10}$$

where $J(u)$ is a Jacobian matrix with u parameters, and $\Gamma = [f_{contact,L}, f_{contact,R}]^T$. Assuming that the instant center of rotation(ICR) does not change for the same terrain, the Jacobian can be expressed as

$$J(\sigma_L, \sigma_R, \delta_x, \delta_{y,R}, \delta_{y,L}) = \frac{2\pi r}{\delta_{y,L} - \delta_{y,R}} \begin{bmatrix} -\delta_{y,R} & \delta_{y,L} \\ \delta_x & -\delta_x \\ -1 & 1 \end{bmatrix} \begin{bmatrix} \sigma_L & 0 \\ 0 & \sigma_R \end{bmatrix} \tag{11}$$

where $\sigma_L, \sigma_R \in [0, 1]$ are slip parameters that account for mechanical effects of the wheel, δ_x is the distance from the robot's local frame to the line which the ICRs' lie on, and $\delta_{y,R}, \delta_{y,L}$ are the y-coordinates of left and right ICRs', respectively.

Eq.11 suggests that as the contact frequency ratio increases, the radius of the turn decreases. We can see that solutions $\{4\}$, $\{5\}$ and $\{6\}$ in Table I have significantly higher frequency ratios than others and correspondingly smaller radii. Although the difference is not significant, similar results are seen between solutions $\{1\}$ and $\{2\}$, where a larger contact frequency ratio results in a smaller turning radius. However, the same comparison cannot be made for $\{4\}$ and $\{5\}$. This might be related to dynamics or ground forces. Nonetheless, solution $\{5\}$ is an outlier in the turning gait library. Another parameter that seems to affect the turning radius is the magnitude of frequencies f_L and f_R used. Despite having the same contact frequency ratio of 2.00, solutions $\{2\}$ and $\{3\}$ have more than a 10% difference in radius. Moreover, the solution with the lower contact frequency has a smaller radius, suggesting lateral slipping in solution $\{2\}$. Unfortunately, as a result of the dual frequency gait cycle method, the robot moves in a way such that contact stability is not continuous. Therefore, assumptions of the extended differential-drive model may not be fully applicable, and more in-depth analysis is needed.

V. Conclusion and Future Work

In this paper, we introduced a novel dual frequency gait planning method that allows QuadRunner, a legged-wheeled robot to turn without any additional turning mechanism onboard. It achieves this by dividing its wheel area into two zones and applying different frequencies. This way, the total contact duration of the same gait cycle can be increased to provide better stability. QuadRunner successfully shows that it can turn with different radii with minimal position errors, increasing its maneuverability for different scenarios. Several experiments were conducted to show the capabilities of our method in depth, and a gait verification was done to ensure the desired cycle was executed. Now, QuadRunner can navigate on flat terrain with both wheeled and legged locomotion to accomplish more complex problems such as payload transfer and manipulation, which will be worked on in the future.

VI. Acknowledgment

The authors gratefully acknowledge the support of the Growth Plan Grant for Aviation and Temasek Laboratories at Singapore University of Technology and Design.

References

[1] R. P. M. Chan, K. A. Stol, and C. R. Halkyard, "Review of modelling and control of two-wheeled robots," *Annual Reviews in Control*, vol. 37, no. 1, pp. 89–103, 2013.

[2] L. Bruzzone and G. Quaglia, "Review article: locomotion systems for ground mobile robots in unstructured environments, mech. sci., 3, 49–62," 2012.
[3] D. Baril, V. Grondin, S.-P. Deschênes, J. Laconte, M. Vaidis, V. Kubelka, A. Gallant, P. Giguere, and F. Pomerleau, "Evaluation of skid-steering kinematic models for subarctic environments," in *2020 17th Conference on Computer and Robot Vision (CRV)*, pp. 198–205, IEEE, 2020.
[4] C. Robotics, "Husky unmanned ground vehicle," *https://clearpathrobotics.com/husky-unmanned-ground-vehicle-robot/*, 2022.
[5] Y. Zhao and S. L. BeMent, "Kinematics, dynamics and control of wheeled mobile robots," in *Proceedings 1992 IEEE International Conference on Robotics and Automation*, pp. 91–92, IEEE Computer Society, 1992.
[6] H.-S. Shim, J.-H. Kim, and K. Koh, "Variable structure control of nonholonomic wheeled mobile robot," in *Proceedings of 1995 IEEE International Conference on Robotics and Automation*, vol. 2, pp. 1694–1699, IEEE, 1995.
[7] A. O. Pullin, N. J. Kohut, D. Zarrouk, and R. S. Fearing, "Dynamic turning of 13 cm robot comparing tail and differential drive," in *2012 IEEE International Conference on Robotics and Automation*, pp. 5086–5093, IEEE, 2012.
[8] W. Guo, J. Qiu, X. Xu, and J. Wu, "Talbot: A track-leg transformable robot," *Sensors*, vol. 22, no. 4, p. 1470, 2022.
[9] U. Saranli, M. Buehler, and D. E. Koditschek, "Rhex: A simple and highly mobile hexapod robot," *The International Journal of Robotics Research*, vol. 20, no. 7, pp. 616–631, 2001.
[10] W.-H. Chen, H.-S. Lin, Y.-M. Lin, and P.-C. Lin, "Turboquad: A novel leg–wheel transformable robot with smooth and fast behavioral transitions," *IEEE Transactions on Robotics*, vol. 33, no. 5, pp. 1025–1040, 2017.
[11] W. Reid, A. H. Göktogan, and S. Sukkarieh, "Moving mammoth: Stable motion for a reconfigurable wheel-on-leg rover," in *Proceedings of Australasian Conference on Robotics and Automation*, pp. 1–10, 2014.
[12] F. Cordes, F. Kirchner, and A. Babu, "Design and field testing of a rover with an actively articulated suspension system in a mars analog terrain," *Journal of Field Robotics*, vol. 35, no. 7, pp. 1149–1181, 2018.
[13] A. A. Hayat, K. Elangovan, M. Rajesh Elara, and M. S. Teja, "Tarantula: Design, modeling, and kinematic identification of a quadruped wheeled robot," *Applied Sciences*, vol. 9, no. 1, p. 94, 2018.
[14] Y. Xue, X. Yuan, Y. Wang, Y. Yang, S. Lu, B. Zhang, J. Lai, J. Wang, and X. Xiao, "Lywal: a leg-wheel transformable quadruped robot with picking up and transport functions," in *2021 IEEE International Conference on Robotics and Automation (ICRA)*, pp. 2935–2941, IEEE, 2021.
[15] J.-J. Chou and L.-S. Yang, "Innovative design of a claw-wheel transformable robot," in *2013 IEEE International Conference on Robotics and Automation*, pp. 1337–1342, IEEE, 2013.
[16] K. Yamamoto and T. Aoki, "Development of novel mobile robot with semicircular wheels," *ROBOMECH Journal*, vol. 7, no. 1, pp. 1–11, 2020.
[17] A. Yeldan, A. Arora, and G. S. Soh, "Quadrunner: A transformable quasi-wheel quadruped," in *2022 International Conference on Robotics and Automation (ICRA)*, pp. 4694–4700, IEEE, 2022.
[18] M. Hildebrand, "The quadrupedal gaits of vertebrates," *Bioscience*, vol. 39, no. 11, p. 766, 1989.
[19] A. Mandow, J. L. Martinez, J. Morales, J. L. Blanco, A. Garcia-Cerezo, and J. Gonzalez, "Experimental kinematics for wheeled skid-steer mobile robots," in *2007 IEEE/RSJ international conference on intelligent robots and systems*, pp. 1222–1227, IEEE, 2007.